LETTER

doi:10.1038/nature26145

Climatic control of Mississippi River flood hazard amplified by river engineering

Samuel E. Munoz[1,2,3], Liviu Giosan[1], Matthew D. Therrell[4], Jonathan W. F. Remo[5], Zhixiong Shen[6,7], Richard M. Sullivan[1,8], Charlotte Wiman[1], Michelle O'Donnell[1] & Jeffrey P. Donnelly[1]

Over the past century, many of the world's major rivers have been modified for the purposes of flood mitigation, power generation and commercial navigation[1]. Engineering modifications to the Mississippi River system have altered the river's sediment levels and channel morphology[2], but the influence of these modifications on flood hazard is debated[3–5]. Detecting and attributing changes in river discharge is challenging because instrumental streamflow records are often too short to evaluate the range of natural hydrological variability before the establishment of flood mitigation infrastructure. Here we show that multi-decadal trends of flood hazard on the lower Mississippi River are strongly modulated by dynamical modes of climate variability, particularly the El Niño–Southern Oscillation and the Atlantic Multidecadal Oscillation, but that the artificial channelization (confinement to a straightened channel) has greatly amplified flood magnitudes over the past century. Our results, based on a multi-proxy reconstruction of flood frequency and magnitude spanning the past 500 years, reveal that the magnitude of the 100-year flood (a flood with a 1 per cent chance of being exceeded in any year) has increased by 20 per cent over those five centuries, with about 75 per cent of this increase attributed to river engineering. We conclude that the interaction of human alterations to the Mississippi River system with dynamical modes of climate variability has elevated the current flood hazard to levels that are unprecedented within the past five centuries.

Flooding of the lower Mississippi River in the spring of 2011 was among the largest discharge events since systematic measurements began in the late nineteenth century, and it caused US$3.2 billion in agricultural losses and damages to infrastructure[6]. This and other recent flood events on the Mississippi River—including those in 2016 and 2017—have repeatedly, although controversially, been attributed to an aggressive campaign of river engineering designed and implemented over the past 150 years[3–5]. Federally mandated efforts to reduce the impacts of flooding began in the late nineteenth century and initially relied almost exclusively on the use of artificial levees, but this strategy was revised in the wake of a particularly devastating flood in the spring of 1927 that overwhelmed the levee system[7]. The current flood management system—the Mississippi River & Tributaries Project (MR&T)—includes a series of spillways that can be opened to relieve pressure on an enlarged levee system, as well as an artificially shortened and straightened main channel that is held in place by concrete retaining walls (revetments) and isolated from most of its natural floodplain[2,6,7]. Although these modifications are credited with protecting communities and croplands within the floodplain from inundation, artificial channelization has altered the relationship between discharge and river stage[3,4] and accelerated the rate of land loss in the Mississippi River delta[8], necessitating additional investments in flood mitigation infrastructure and coastal restoration[9].

Although fluvial processes are sensitive to flood mitigation infrastructure, climate variability can also shape the dynamics of continental drainage networks, particularly over decadal to centennial timescales that are difficult to detect using short observational records[10,11]. Precipitation and soil water storage over the Mississippi River basin are influenced by climate variability driven by sea-surface-temperature anomalies in both the Pacific and Atlantic Oceans[12,13]. Yet establishing the natural controls on discharge extremes of the lower Mississippi has proved challenging because gauging-station measurements record a limited range of variability, particularly before major investments were made in river engineering. As a result, analyses of historical streamflow records disagree over the role that dynamical modes of climate variability play in modulating the discharge[12,14,15]. To plan flood mitigation and other infrastructure projects, it is critical to understand the climate controls on the discharge of the lower Mississippi River, but the short length of the instrumental record limits our ability to evaluate the range of natural hydrological variability from observational data alone.

Recent advances in palaeoflood hydrology could extend the instrumental record back in time to diagnose the controls on the discharge of large alluvial rivers such as the lower Mississippi. Traditional approaches in palaeoflood hydrology, which include the use of slackwater deposits as flood event indices[16], are of limited use on the low-relief landscapes that characterize the Mississippi River alluvial plain. One new approach uses the sedimentary archives held in floodplain lakes, which act as sediment traps during overbank floods, to develop continuous, quantitative and event-scale records of past flood frequency and magnitude[17,18]. Parallel work in dendrochronology demonstrates that when trees are inundated by floodwaters they exhibit anatomical anomalies in that year's growth ring such that they provide a precise chronology of flood events that occurred during the growing season[19]. Together, these methodological advances provide an opportunity to evaluate interannual to multi-decadal scale trends in flood frequency and magnitude on a large alluvial river such as the lower Mississippi, before and during the era of river engineering.

Here we analyse records of individual overbank flood events derived from sedimentary and tree-ring archives from the lower Mississippi River's floodplain (Fig. 1). We collected sediment cores from the infilling thalwegs of three oxbow lakes, Lake Mary (MRY), False River Lake (FLR) and Lake Saint John (STJ), that formed by neck cut-offs of the lower Mississippi River in AD 1776, AD 1722 and roughly AD 1500, respectively[20] (Extended Data Figs 1–3). In these sedimentary archives, we identified individual flood events by using grain-size analysis, bulk geochemistry (from X-ray fluorescence scanning, XRF) and radiography; developed age–depth models constrained by multiple independent chronological controls (Extended Data Figs 4–6); and estimated flood magnitudes from a linear model that relates the coarse

[1]Department of Geology & Geophysics, Woods Hole Oceanographic Institution, Woods Hole, Massachusetts 02543, USA. [2]Marine Science Center, Department of Marine & Environmental Sciences, Northeastern University, Nahant, Massachusetts 01908, USA. [3]Department of Civil & Environmental Engineering, Northeastern University, Boston, Massachusetts 02115, USA. [4]Department of Geography, University of Alabama, Tuscaloosa, Alabama 35401, USA. [5]Department of Geography and Environmental Resources, Southern Illinois University, Carbondale, Illinois 62901, USA. [6]Department of Marine Sciences, Coastal Carolina University, Conway, South Carolina 29526, USA. [7]Department of Geography and Planning, University of Liverpool, Liverpool L69 7ZT, UK. [8]Department of Oceanography, Texas A&M University, College Station, Texas 77840, USA.

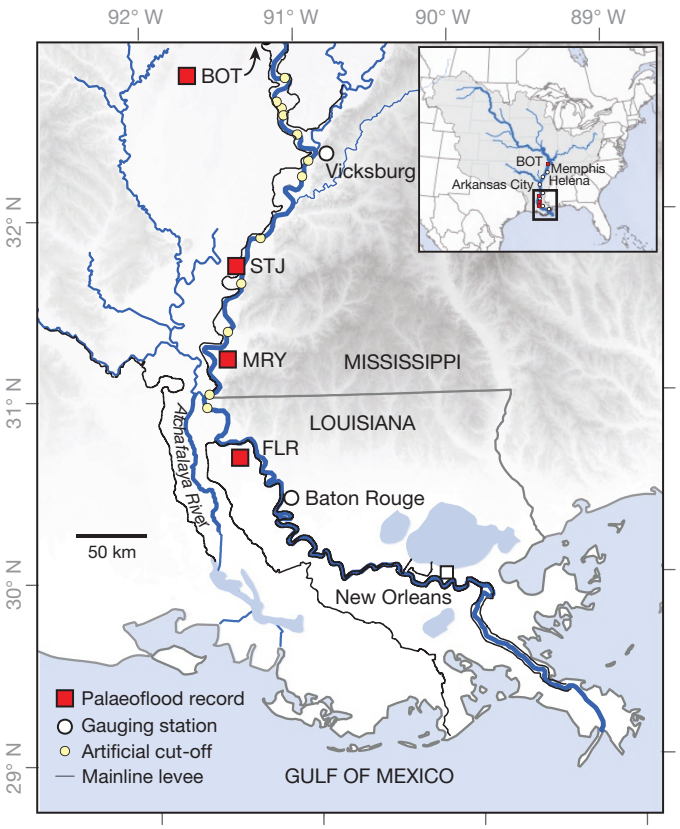

Figure 1 | The lower Mississippi River and the Mississippi River basin in North America. River engineering modifications (artificial cut-offs and levees) that contribute to channelization, the locations of palaeoflood records (FLR; MRY; STJ; and Big Oak Tree, BOT) and river gauging stations on the lower Mississippi used in this study (Memphis, Helena, Arkansas City, Vicksburg and Baton Rouge) are shown. Shaded relief shows relative topographic highs (dark shades) and lows (light shades) using the National Elevation Dataset[25].

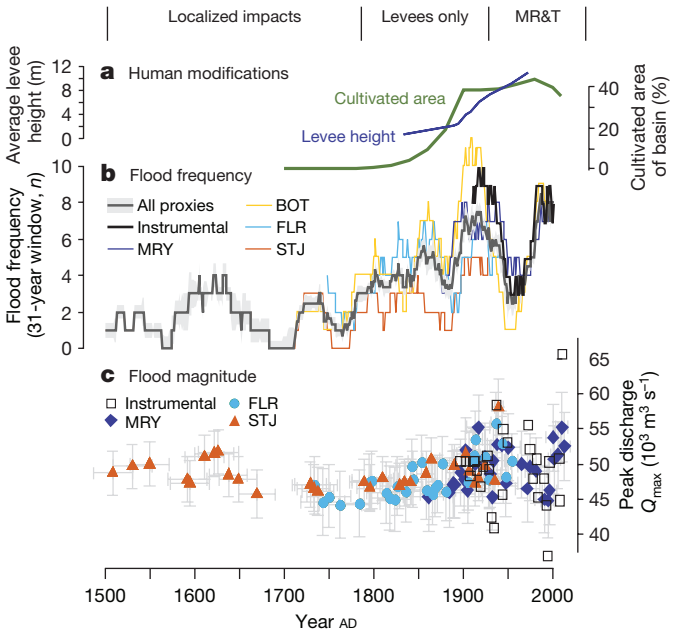

Figure 2 | Instrumental and reconstructed flood frequencies and magnitudes of the lower Mississippi River. a, Human impacts to the lower Mississippi River (MR&T refers to a major river engineering initiative): timing and intensity of agricultural land use[26] and river engineering. **b**, Flood frequencies (number of flood events in a 31-year moving window) derived from palaeoflood records, including mean and bootstrapped 2σ confidence intervals of all palaeoflood archives, and the instrumental frequency of all floods attaining major flood stage (>1.5 m above flood stage) at the Mississippi River gauging station at Baton Rouge (station number 07374000). **c**, Flood magnitudes derived from the sedimentary palaeoflood records, with 1σ uncertainties, and instrumental flood magnitudes for the Mississippi River gauging station at Vicksburg (station number 07289000).

grain-size component to the discharge of historical flood events[18] (Extended Data Fig. 7; see Methods for details). We also include tree-ring records from the floodplain of the lower Mississippi, collected and described by ref. 21; each tree-ring series was examined for anatomical evidence of flood injury to produce a record of overbank flood events that extends back to the late seventeenth century[21]. A composite time series for flood frequency describing the number of flood events in a moving 31-year window derived from sedimentary and tree-ring archives (Fig. 2b) is highly correlated with instrumental flood frequency ($r = 0.90$, $t = 19.12$, effective degrees of freedom $\nu_{eff} = 3.77$, $p < 0.001$) for the interval of overlap, while reconstructed flood magnitudes (Fig. 2c) track trends observed in gauging-station measurements (see Supplementary Information for additional validation), indicating that the palaeoflood archives provide robust reconstructions of hydrological extremes on the lower Mississippi River beyond the period of instrumental record.

Our multi-proxy palaeoflood dataset extends the record of extremes in the discharge of the lower Mississippi River back to the early sixteenth century and demonstrates that both the frequency and magnitude of flooding have increased over the past 150 years as land use and river engineering efforts have intensified (Fig. 2). Flood frequencies and magnitudes exhibit multi-decadal oscillations that increase in amplitude around the beginning of the twentieth century such that the highest rates of overbank flooding and the largest discharge events of the past 500 years have occurred within the past century. The amplification of flood magnitudes that has occurred over the past 150 years corresponds in time with the intensification of anthropogenic modifications to the lower Mississippi River and its basin, particularly the artificial channelization of the river with levees, revetments and cut-offs in the late nineteenth and early twentieth centuries[2,7]. Yet the continued presence of multi-decadal oscillations in flood frequency and magnitude throughout the entire period of record indicates that anthropogenic modifications to the Mississippi River system are acting in concert with other factors to alter flood hazard through time.

To evaluate the role of climate variability on flood hazard, we examined the relationships between flood frequency, the El Niño–Southern Oscillation (ENSO) and the Atlantic Multidecadal Oscillation (AMO), to find that sea-surface temperature anomalies in both the Pacific and Atlantic Oceans exert a strong influence on the occurrence of lower Mississippi River floods (Fig. 3). Over the past five centuries, correlations between composite flood frequency and the frequency of El Niño events ($r = 0.73$) and the AMO index ($r = -0.39$) derived from instrumental and palaeoclimate data sets are significant ($p < 0.001$; see Methods for details). The strength and direction of these relationships support the hypothesis that discharge extremes on the lower Mississippi River arise through the interaction of ENSO, which influences antecedent soil moisture, with the AMO, which controls the flux of moisture from the Gulf of Mexico inland[12,15]. Extreme precipitation events over the Mississippi River basin are associated with a stronger and more westerly position of the North Atlantic Subtropical High that is characteristic of the negative phase of the AMO[12,13], and these heavy precipitation events are more likely to generate discharge extremes if they fall on the saturated soils that tend to be left in the wake of El Niño events[15].

Despite the strong influence of climatic variability on lower Mississippi River flood occurrence, the amplification of flood magnitudes that we observe over the past 150 years is primarily the result of human modifications to the river and its basin (Fig. 4). The magnitude

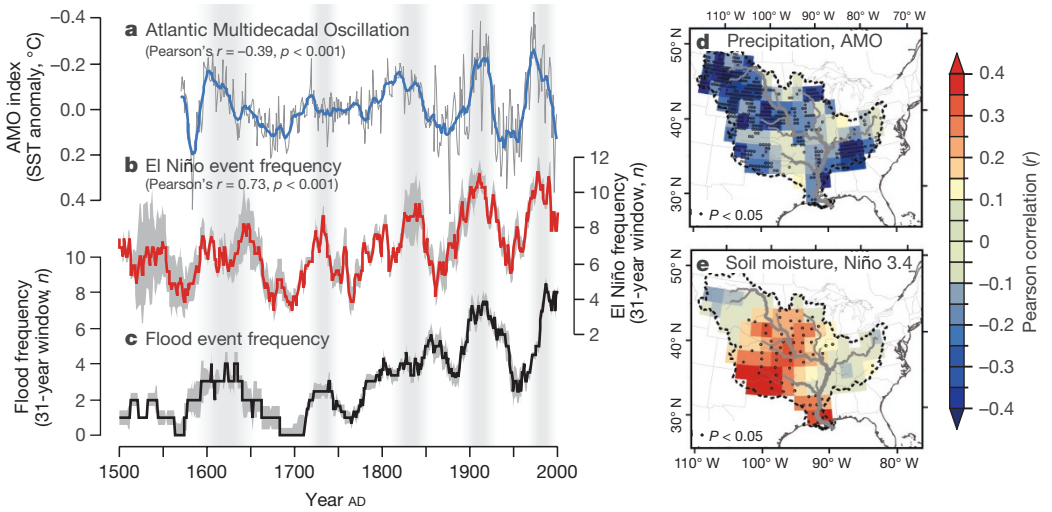

Figure 3 | Lower Mississippi River flood frequency and its relation to dominant modes of climate variability. a, AMO derived from instrumental[27] and palaeoclimate[28] datasets. **b**, Frequency of El Niño events (the warm phase of the ENSO) in a 31-year moving window derived from instrumental[27] and palaeoclimate[28–31] data sets (mean with 2σ bootstrapped confidence interval). SST, sea surface temperature. **c**, Frequency of lower Mississippi River floods derived from palaeoflood data (mean with bootstrapped 2σ confidence interval). **d**, Correlation field of monthly precipitation[32] with the AMO[27] (AD 1901–2014) smoothed with a common 121-month filter. **e**, Correlation field of monthly Palmer Drought Severity Index[33] with the Niño 3.4 index[27] (AD 1948–2011). Correlation fields are interpolated to a common 2° × 2° grid, and individual points with significant correlations at the $P < 0.05$ level are marked with a hollow circle.

of the 100-year flood (Q_{100}; a flood with a 1% chance of exceedance in any year) estimated from gauging-station measurements (AD 1897–2015) is (20 ± 7)% larger than Q_{100} for the period before major human impacts to the river and its basin (AD 1500–1800), as estimated from the palaeoflood data (see Methods for details). To identify the influence of human activities on this observed increase in Q_{100}, we use a linear model that relates peak discharge to the AMO index over the period before major human impacts to the river, AD 1500–1800 ($R^2 = 0.35$, degrees of freedom $\nu = 18$, $p < 0.01$) and use this model to predict flood magnitudes over the entire period of record. This 'climate-only' regression predicts that, in the absence of human modifications to the land surface, Q_{100} would have increased by only (5 ± 6)% over the same period, accounting for only about 25% of the observed increase in Q_{100} and implying that the remainder (about 75%) of this elevated flood hazard is the result of human modifications to the river and its basin.

The timing and nature of the amplification of flood magnitudes at the onset of the twentieth century strongly imply that it reflects the transformation of a freely meandering alluvial river to an artificially confined channel, because the confinement of flood flows to a levee-defined floodway can speed up the downstream propagation of a flood wave and increase peak discharge for a given flood[22]. The establishment of widespread agricultural activity in the Mississippi River basin occurred in the nineteenth century, before the divergence of the observed and 'climate-only' flood magnitudes, indicating a secondary and possibly lagged influence of agricultural expansion[23] on flood magnitudes relative to that of river engineering. In short, this analysis identifies artificial channelization of the lower Mississippi River, and its effects on the river's gradient, channel area and flow velocity[2,7], as having significantly increased the discharge of a given flood event relative to pre-engineering conditions.

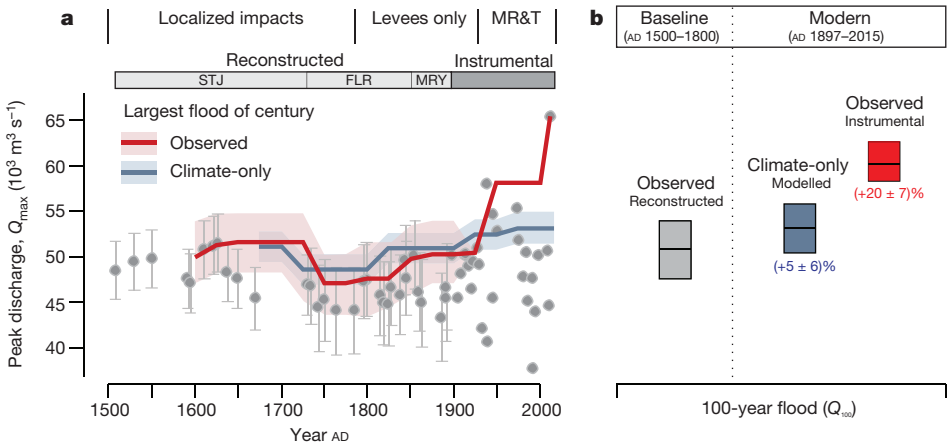

Figure 4 | Attribution of the observed increase in flood magnitudes over the past five centuries. a, Composite peak discharges from palaeoflood archives and the instrumental record from Vicksburg. The red line indicates observed trends in the largest flood of the century in a moving window; the blue line indicates trends under 'climate-only' conditions, estimated from a statistical model (see text for details). Both lines are shown with 1σ confidence intervals. Instrumental peak discharge estimates are reported without uncertainty and are therefore plotted without confidence intervals. **b**, Comparison of the 100-year flood observed during the baseline period (AD 1500–1800, before major human modifications to the Mississippi River and its basin; grey boxplot) with that estimated using a statistical model under 'climate-only' conditions (blue boxplot) and observed (red boxplot) during the modern period of instrumental record (AD 1897–2015). Boxplots show mean (centre line) and 1σ confidence intervals (box top and bottom) for Q_{100} estimates.

Our main finding—that river engineering has elevated flood hazard on the lower Mississippi to levels that are unprecedented within the past five centuries—adds to a growing list of externalized costs associated with conventional flood mitigation and navigation projects, including a reduction in a river's ability to convey flood flows[3,4], the acceleration of coastal land loss[8] and hypoxia[24]. Despite the societal benefits that these major infrastructure projects convey[6], the costs associated with maintaining current levels of flood protection and navigability will continue to grow at the expense of communities and industries situated in the river's floodplain and its delta. For those interested in improving seasonal and longer-term forecasts of flood hazard or management strategies that reconnect the river with its floodplain, the Mississippi River's discharge of freshwater—and by extension the flux of sediment, nutrients and pollutants—to its outlet should be viewed as highly sensitive both to anthropogenic modifications to the basin and to variability of the global climate system.

Online Content Methods, along with any additional Extended Data display items and Source Data, are available in the online version of the paper; references unique to these sections appear only in the online paper.

Received 27 June 2017; accepted 31 January 2018.

1. Meybeck, M. Global analysis of river systems: from Earth system controls to Anthropocene syndromes. *Phil. Trans. R. Soc. Lond. B* **358,** 1935–1955 (2003).
2. Smith, L. M. & Winkley, B. R. The response of the lower Mississippi River to river engineering. *Eng. Geol.* **45,** 433–455 (1996).
3. Criss, R. E. & Shock, E. L. Flood enhancement through flood control. *Geology* **29,** 875–878 (2001).
4. Pinter, N., Jemberie, A. A., Remo, J. W., Heine, R. A. & Ickes, B. S. Flood trends and river engineering on the Mississippi River system. *Geophys. Res. Lett.* **35,** L23404 (2008).
5. Watson, C. C., Biedenharn, D. S. & Thorne, C. R. Analysis of the impacts of dikes on flood stages in the Middle Mississippi River. *J. Hydraul. Eng.* **139,** 1071–1078 (2013).
6. Camillo, C. A. *Divine Providence: The 2011 Flood in the Mississippi River and Tributaries Project* (Mississippi River Commission, 2012).
7. Remo, J. W. F. *Fishery Resources, Environment, and Conservation in the Mississippi and Yangtze (Changjiang) River Basins* Ch. 11 (American Fisheries Society, 2016).
8. Blum, M. D. & Roberts, H. H. Drowning of the Mississippi Delta due to insufficient sediment supply and global sea-level rise. *Nat. Geosci.* **2,** 488–491 (2009).
9. Louisiana Coastal Protection and Restoration Authority. *Louisiana's Comprehensive Master Plan for a Sustainable Coast* (Coastal Protection and Restoration Authority of Louisiana, 2017).
10. Aalto, R. *et al.* Episodic sediment accumulation on Amazonian flood plains influenced by El Niño/Southern Oscillation. *Nature* **425,** 493–497 (2003).
11. Darby, S. E. *et al.* Fluvial sediment supply to a mega-delta reduced by shifting tropical-cyclone activity. *Nature* **539,** 276–279 (2016).
12. Enfield, D. B., Mestas-Nuñez, A. M. & Trimble, P. J. The Atlantic multidecadal oscillation and its relation to rainfall and river flows in the continental US. *Geophys. Res. Lett.* **28,** 2077–2080 (2001).
13. Hu, Q., Feng, S. & Oglesby, R. J. Variations in North American summer precipitation driven by the Atlantic Multidecadal Oscillation. *J. Clim.* **24,** 5555–5570 (2011).
14. Rogers, J. C. & Coleman, J. S. Interactions between the Atlantic Multidecadal Oscillation, El Niño/La Niña, and the PNA in winter Mississippi valley stream flow. *Geophys. Res. Lett.* **30,** (2003).
15. Munoz, S. E. & Dee, S. G. El Niño increases the risk of lower Mississippi River flooding. *Sci. Rep.* **7,** https://doi.org/10.1038/s41598-017-01919-6 (2017).
16. Baker, V. R. Paleoflood hydrology and extraordinary flood events. *J. Hydrol.* **96,** 79–99 (1987).
17. Munoz, S. E. *et al.* Cahokia's emergence and decline coincided with shifts of flood frequency on the Mississippi River. *Proc. Natl Acad. Sci. USA* **112,** 6319–6324 (2015).
18. Toonen, W. H. J., Winkels, T. G., Cohen, K. M., Prins, M. A. & Middelkoop, H. Lower Rhine historical flood magnitudes of the last 450 years reproduced from grain-size measurements of flood deposits using end member modelling. *Catena* **130,** 69–81 (2015).
19. St. George, S. & Nielsen, E. Signatures of high-magnitude nineteenth-century floods in *Quercus macrocarpa* tree rings along the Red River, Manitoba, Canada. *Geology* **28,** 899–902 (2000).
20. Fisk, H. N. *Geological Investigation of the Alluvial Valley of the Lower Mississippi River* (Mississippi River Commission, 1945)
21. Therrell, M. D. & Bialecki, M. B. A multi-century tree-ring record of spring flooding on the Mississippi River. *J. Hydrol.* **529,** 490–498 (2015).
22. Jacobson, R. B., Lindner, G. & Bitner, C. The role of floodplain restoration in mitigating flood risk, lower Missouri River, USA. *Geomorphic Approaches to Integrated Floodplain Management of Lowland Fluvial Systems in North America and Europe* 203–243 (Springer, 2015).
23. Trimble, S. W. Decreased rates of alluvial sediment storage in the Coon Creek Basin, Wisconsin, 1975–93. *Science* **285,** 1244–1246 (1999).
24. Rabalais, N. N. *et al.* Dynamics and distribution of natural and human-caused hypoxia. *Biogeosciences* **7,** 585–619 (2010).
25. Gesch, D. *et al.* The National Elevation Dataset. *Photogramm. Eng. Remote Sensing* **68,** 5–32 (2002).
26. Klein Goldewijk, K., Beusen, A., Doelman, J. & Stehfest, E. New anthropogenic land use estimates for the Holocene; HYDE 3.2. *Earth Syst. Sci. Data Discuss.* https:doi.org/10.5194/essd-2016-58 (2016).
27. Rayner, N. A. *et al.* Global analyses of sea surface temperature, sea ice, and night marine air temperature since the late nineteenth century. *J. Geophys. Res. Atmos.* **108,** 4407 (2003).
28. Braganza, K., Gergis, J. L., Power, S. B., Risbey, J. S. & Fowler, A. M. A multiproxy index of the El Niño–Southern Oscillation, AD 1525–1982. *J. Geophys. Res. Atmos.* **114,** D05106 (2009).
29. Gergis, J. L. & Fowler, A. M. A history of ENSO events since AD 1525: implications for future climate change. *Clim. Change* **92,** 343–387 (2009).
30. Li, J. *et al.* Interdecadal modulation of El Niño amplitude during the past millennium. *Nat. Clim. Chang.* **1,** 114–118 (2011).
31. McGregor, S., Timmermann, A. & Timm, O. A unified proxy for ENSO and PDO variability since 1650. *Clim. Past* **6,** 1–17 (2010).
32. Schneider, U. *et al.* Evaluating the hydrological cycle over land using the newly-corrected precipitation climatology from the Global Precipitation Climatology Centre (GPCC). *Atmosphere* **8,** 52–69 (2017).
33. Vose, R. S. *et al.* Improved historical temperature and precipitation time series for U.S. climate divisions. *J. Appl. Meteorol. Climatol.* **53,** 1232–1251 (2014).

Supplementary Information is available in the online version of the paper.

Acknowledgements We thank S. Colman, S. G. Dee, K. Lotterhos, S. P. Muñoz, W. H. J. Toonen, G. C. Trussell and T. Webb III for discussion and comments, and M. Besser, D. Carter, J. Elsenbeck, K. Esser, A. LaBella and J. Nienhuis for field and/or laboratory assistance. Seed funding for this project was provided to L.G. and J.P.D. by the Coastal Ocean Institute of WHOI. Support for S.E.M. was provided by the Postdoctoral Scholar Program of the Woods Hole Oceanographic Institution (WHOI). Additional support to S.E.M. and L.G. was provided by the Ocean and Climate Change Institution of WHOI. Support for M.D.T. and J.W.F.R. was provided by the US National Science Foundation Geography and Spatial Science Program (award number BSC1359801). This is contribution no. 362 from the Marine Science Center at Northeastern University.

Author Contributions L.G. and J.P.D. initiated the project. S.E.M., L.G., M.D.T., J.W.F.R., Z.S. and J.P.D. conceived the ideas, designed the study and interpreted the results. M.D.T. provided dendrochronological data. J.W.F.R. provided historical discharge and geospatial data. Z.S. performed OSL dating. S.E.M., L.G., R.M.S., C.W. and M.O. collected sedimentary archives and/or performed laboratory analyses. S.E.M. wrote the manuscript with contributions from all authors.

Author Information Reprints and permissions information is available at www.nature.com/reprints. The authors declare no competing interests. Readers are welcome to comment on the online version of the paper. Publisher's note: Springer Nature remains neutral with regard to jurisdictional claims in published maps and institutional affiliations. Correspondence and requests for materials should be addressed to S.E.M. (s.munoz@northeastern.edu).

Reviewer Information *Nature* thanks P. Hudson, S. St George and the other anonymous reviewer(s) for their contribution to the peer review of this work.

METHODS

Instrumental streamflow data. We obtained daily stage data for Mississippi River gauges at Vicksburg (station number 07289000) and Baton Rouge (07374000) from the United States Army Corps of Engineers (USACE) and the United States Geological Survey (USGS). Discharges for the Vicksburg, Memphis (07032000), Helena (07047970), Arkansas City (07146500) and Baton Rouge gauges were compiled from multiple sources. For the early instrumental record (pre-1927), peak discharges and measured discharges were compiled from historical documents[34,35]. In the few cases in which annual peak discharges were not recorded during this period, we used the measured discharges to create rating curves from which to determine the peak discharge for the annual peak stage. Discharge data after AD 1927 were acquired either from the USACE or from the USGS. The discharge record at Vicksburg is the longest and most continuous of the available discharge records, and its peak annual discharge is highly correlated ($r > 0.86$, $p < 0.01$) with that of other lower Mississippi River gauging stations in the study area (see Supplementary Information) and was thus used to reconstruct flood magnitudes from the sedimentary archives.

Sedimentary archives. We collected sediment cores from the infilling thalwegs of MRY, FLR and STJ with a rod-driven vibracore system in July 2012 and March 2016 (Extended Data Figs 1–3). For each core, we collected a replicate drive using a 7.5-cm-diameter polycarbonate piston corer to ensure recovery of an intact sediment/water interface. The targeted lakes were selected because the lateral position of the active channel near the lake's arm has remained relatively stable from the time of cut-off to the mid-twentieth century[20]. We cannot eliminate the possibility that minor lateral and/or vertical channel migration has occurred near these lakes since the time of cut-off, but we reduce the influence of this potential bias on our analysis by (i) using a low-pass filter on the grain-size data (see below) and (ii) validating the resulting flood frequency and magnitude data sets against the instrumental record (see Supplementary Information). At FLR and STJ, mainline levees of the MR&T have inhibited the deposition of fluvial sediment in the lake during overbank floods after about AD 1950 and 1937, respectively; MRY is not protected by artificial levees and it continues to be inundated during overbank floods. Oxbow lakes can continue to exchange water and sediment with the main channel when the river is below flood stage[36] to create high rates of fine-grained 'background sedimentation' that differs in texture and composition from the coarser material that is mobilized during high-magnitude flood events. Cores were collected along an arm of the oxbow lakes at locations proximal to the 'plug' that separates the active channel from the lake to maximize the contrast between background and flood event sediments. Core locations at each site were targeted based on bathymetric surveys before core collection.

Cores were transported back to the Woods Hole Oceanographic Institution (WHOI) where they were split, described and photographed. Archived core halves were subjected to high-resolution XRF (4,000 μm resolution) and radiography (200 μm resolution) in an ITRAX core scanner housed at WHOI. For grain-size analysis, sediment sub-samples at continuous 1-cm intervals were dispersed in water using a vortex mixer before 5 s sonication and analysis in a Beckman Coulter LS 13 320 laser diffraction particle-size analyser; randomly selected replicate samples showed a <1% volume difference in any detector. Complex, multi-modal grain-size distributions were modelled as mixtures of discrete, simple distributions and decomposed using end-member calculations into four representative populations, or end-members (EMs), that were considered geologically meaningful, using the EMMAgeo package run in RStudio. The score of each sample on the coarsest end-members (EM1), representing deposition of bedload during overbank floods[18], was normalized with a low-pass (41-cm) moving minimum filter to remove long-term trends in sediment composition caused by local geomorphic processes. We then identified potential flood deposits as normalized EM1 scores that exceeded a high-pass (11-cm) moving mean with a 0.1 EM1 score threshold, and we verified identified peaks against the XRF and radiography (Extended Data Figs 4–6).

To estimate flood magnitudes from the sediment records, we used the method of ref. 18 and developed linear models that describe the normalized EM1 scores as a function of historical flood event discharge at the Mississippi River gauging station at Vicksburg. Using this, we assigned each flood deposit to a historical flood event approximating 'major flood stage' as defined by the USGS at a nearby gauging station, in stratigraphic order, and within the 2σ age estimate for the deposit (Extended Data Fig. 7). The requirement for flood deposits to be assigned to historical floods in stratigraphic order eliminated ambiguity in cases in which more than one historical flood fell within a deposit's 2σ age estimate. There were no cases for which a flood deposit could not be assigned to a historical flood within the period of instrumental observations (AD 1897–2015), but there were three cases at FLR (AD 1944, 1929 and 1920) and two cases at STJ (AD 1920 and 1913) for which a major historic flood did not leave an identifiable flood deposit. These 'missing' flood deposits are rare and occurred during periods of high flood frequency, and they may reflect reduced sediment availability[37] during these events. The sedimentary record reconstructs peak annual discharge at the Vicksburg gauge, not at individual site locations.

We developed age–depth models using Bacon v.2.2[38], a Bayesian age–depth modelling program, informed by multiple independent dating techniques (see Supplementary Information), including: (i) ^{137}Cs and ^{210}Pb activity in desiccated and powdered bulk sediment samples in a Canberra GL2020RS well detector for low-energy germanium gamma radiation, for which we used the constant rate of supply model[39] to estimate the age of a sampled depth; (ii) radiocarbon (^{14}C) dating via accelerator mass spectrometry of a terrestrial plant macrofossil at the National Ocean Sciences Accelerator Mass Spectrometers facility at WHOI, calibrated using the IntCal13 curve embedded in Bacon; (iii) optically stimulated luminescence (OSL) dating with the fast component of silt-sized quartz[40] using a Risø DA-15 B/C luminescence reader at the University of Liverpool, UK; (iv) core tops as the date of collection and, when appropriate, the age of lake formation[20] as the core bottom. Sedimentation rate priors were increased to near-instantaneous rates through thick (>20 cm) flood deposits[17].

Tree-ring records. Tree-ring samples from 33 living and 2 dead oak (*Quercus lyrata* and *Q. macrocarpa*) trees were collected from Big Oak Tree State Park (BOT) in southeast Missouri[21]. One to four core samples were extracted from each tree at or below breast height (about 1.4 m) using a 5-mm-diameter Swedish increment borer. Cross-sections from dead trees were collected as close to the base of the tree as possible. All samples were absolutely cross-dated using the skeleton-plot method of dendrochronology. Tree-ring widths were measured on a stage micrometer to a nominal resolution of 0.001 mm. We crosschecked the accuracy of our visual dating using the computer program COFECHA. We visually determined flood-ring years by examining each tree-ring series for any evidence of flood injury consistent with the anomalous anatomical features caused by flooding as described by previous flood-ring studies[19]. Additional characteristics used in our identification included 'jumbled ranks' or 'additional ranks' of early wood vessels or zones of 'extended earlywood' and disorganized flame parenchyma as well as 'offset' early wood ranks[19]. We used the same criteria as ref. 21 to identify flood events (that is, a year in which more than 10% of sampled trees exhibited signs of flood injury) as this threshold encompasses all historic floods that attained major flood stage and occurred during the growing season[21].

Historical climate and palaeoclimate data. Historical (late nineteenth century to present) indices of ENSO and AMO[27] were extended back to the sixteenth century with annual palaeoclimate reconstructions of ENSO[28–31] and AMO[41]. To compare the ENSO series, we identified El Niño events in the historical Niño 3.4 index as periods of five consecutive overlapping 3-month windows at or above +0.5 °C, and as years with anomalies of more than +0.5 °C in the palaeoclimate series. We then derived El Niño event frequencies using a 31-year moving window on each record, and we computed the mean of the historical and all palaeoclimate El Niño frequencies and bootstrapped 2σ confidence intervals using the *boot* function in RStudio. For the composite AMO series, we used the detrended historical AMO index[27] back to AD 1871, and then transitioned to a palaeoclimate AMO reconstruction[41] to AD 1572. We sampled this composite AMO index at the median age probability of the 20 palaeofloods that occurred between AD 1500–1800, and used these data to develop a linear model (using the *lm* function in RStudio) that relates peak discharge from the AMO index; the El Niño frequency timeseries was not a significant predictor of flood magnitudes, presumably because Pacific sea-surface temperatures do not control the inland flux of Gulf of Mexico moisture that triggers high-magnitude discharge events[15], so only the AMO index was used to statistically estimate flood magnitudes under 'climate-only' conditions. The AMO is detrended to remove recent warming of North Atlantic sea surface temperatures, so the 'climate-only' estimates of Q_{100} do not consider the potential effects of recent greenhouse warming on flood magnitudes—although we note that the inverse relationship between AMO and Mississippi River flood magnitudes implies that warming of North Atlantic sea-surface temperatures would act to suppress flood magnitudes. When evaluating the significance of Pearson correlations between climate and hydrological time-series that exhibited high degrees of serial autocorrelation, we estimated the effective degrees of freedom with the following relation[42]:

$$\nu_{\mathrm{eff}} = N(1-\varphi_x\varphi_y)/(1+\varphi_x\varphi_y) \quad (1)$$

where N is the number of independent samples, and φ_x and φ_y are the lag-1 autocorrelation coefficients of time series x and y respectively.

Flood hazard attribution. The magnitude of Q_{100} was estimated both empirically and through statistical modelling. The sedimentary palaeoflood archives record major flood events over periods greater than 100 years, and are suitable for estimating recurrence intervals empirically through the relation:

$$t_{\mathrm{r}} = (n+1)/m \quad (2)$$

where t_r is the recurrence interval (the inverse of t_r is the probability that the event magnitude will be exceeded in any one year), n is the number of years in the window being considered, and m is the number of recorded occurrences of the event being considered. The same approach was used to estimate Q_{100} in the statistically modelled 'climate-only' peak annual discharges derived from palaeoclimate and historical climate records. The instrumental record at the Vicksburg gauge provides a measurement for peak annual discharge in every year, but is relatively short, so the modern Q_{100} was estimated statistically by fitting a log Pearson type III distribution to the data set following standard protocols outlined by the United States Interagency Advisory Committee of Water Data[43] for instrumental hydrological data sets. We compared the observed Q_{100} baseline (AD 1500–1800) with the observed and 'climate-only' Q_{100} estimates for the modern period (AD 1897–2015) and attributed the proportion of the observed change that was not explained by the 'climate-only' estimates to human alterations to the river channel and basin. The modern Q_{100} estimated empirically from sedimentary records and the modern Q_{100} estimated by fitting a generalized extreme value distribution to the instrumental data both fall within the 1σ confidence intervals of the modern Q_{100} estimated by fitting a log Pearson type III to the instrumental record (see Supplementary Information), indicating that our findings are robust to different estimations of flood hazard.

Data availability statement. The datasets generated by this study are available as Supplementary Data.

Code availability. The R code used to produce the figures in this paper is available from the corresponding author on reasonable request.

34. Mississippi River Commission. *Results of the Discharge Observations Mississippi River and its Tributaries and Outlets, 1838–1923* (Mississippi River Commission, 1925).
35. Mississippi River Commission. *Results of the Discharge Observations Mississippi River and its Tributaries and Outlets, 1924–1930* (Mississippi River Commission, 1931).
36. Hudson, P. F., Sounny-Slitine, M. A. & LaFevor, M. A new longitudinal approach to assess hydrologic connectivity: embanked floodplain inundation along the lower Mississippi River. *Hydrol. Processes* **27,** 2187–2196 (2013).
37. Heitmüller, F. T., Hudson, P. F. & Kesel, R. H. Overbank sedimentation from historic ad 2100 flood along the lower Mississippi River, USA. *Geology* **45,** 107–110 (2017).
38. Blaauw, M. & Christen, J. A. Flexible paleoclimate age–depth models using an autoregressive gamma process. *Bayesian Anal.* **6,** 457–474 (2011).
39. Appleby, P. G. & Oldfield, F. The calculation of lead-210 dates assuming a constant rate of supply of unsupported ^{210}Pb to the sediment. *Catena* **5,** 1–8 (1978).
40. Shen, Z. & Lang, A. Quartz fast component optically stimulated luminescence: towards routine extraction for dating applications. *Radiat. Meas.* **89,** 27–34 (2016).
41. Gray, S. T., Graumlich, L. J., Betancourt, J. L. & Pederson, G. T. A tree-ring based reconstruction of the Atlantic Multidecadal Oscillation since 1567 AD. *Geophys. Res. Lett.* **31,** L12205 (2004).
42. Dawdy, D. & Matlas, N. *Statistical and Probability Analysis of Hydrologic Data, Part III: Analysis of Variance, Covariance and Time Series* (McGraw-Hill, 1964).
43. Interagency Advisory Committee on Water Data. *Guidelines for Determining Flood-Flow Frequency: Bulletin 17B of the Hydrology Subcommittee* (United States Geological Survey, 1982).

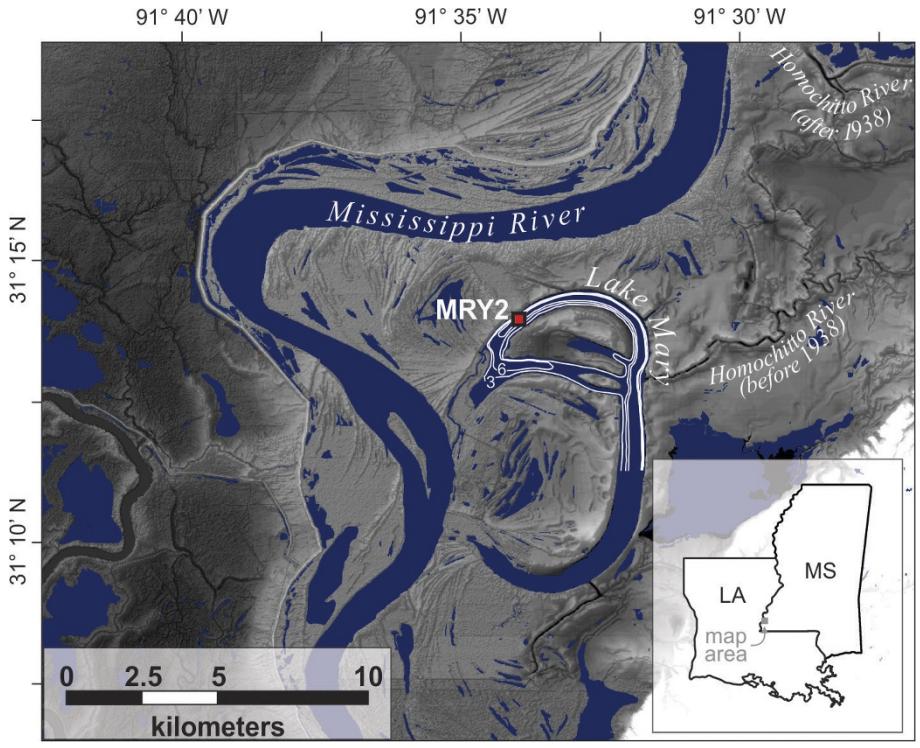

Extended Data Figure 1 | Location of Lake Mary, Mississippi (MRY) and sediment core (MRY2) used in this study. Lake Mary is an oxbow lake that formed via neck cut-off of the lower Mississippi River in AD 1776[20] and is situated inside the modern floodway such that it continues to be inundated during overbank floods. Bathymetric contours (white) given in metres. Shaded relief shows relative topographic lows (dark shades) and highs (light shades) according to the National Elevation Dataset[25].

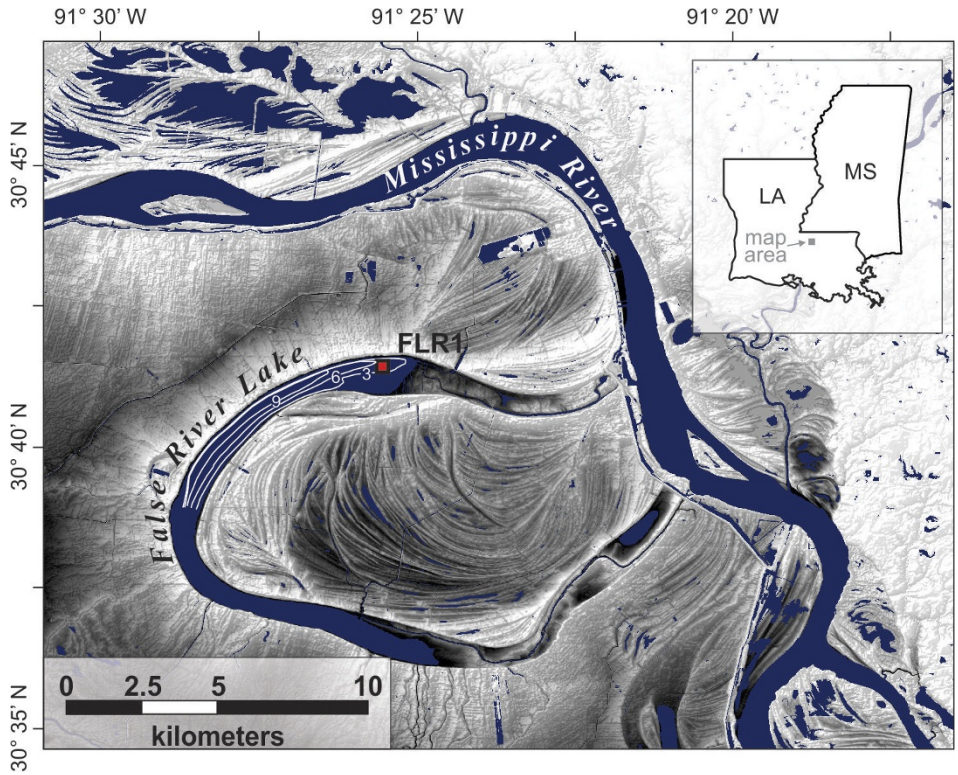

Extended Data Figure 2 | Location of False River Lake, Louisiana, and sediment core (FLR1) used in this study. False River Lake is an oxbow lake that formed via neck cut-off of the lower Mississippi River in AD 1722[20] and is situated outside the modern floodway. Bathymetric contours (white) given in metres. Shaded relief shows relative topographic lows (dark shades) and highs (light shades) according to the National Elevation Dataset[25].

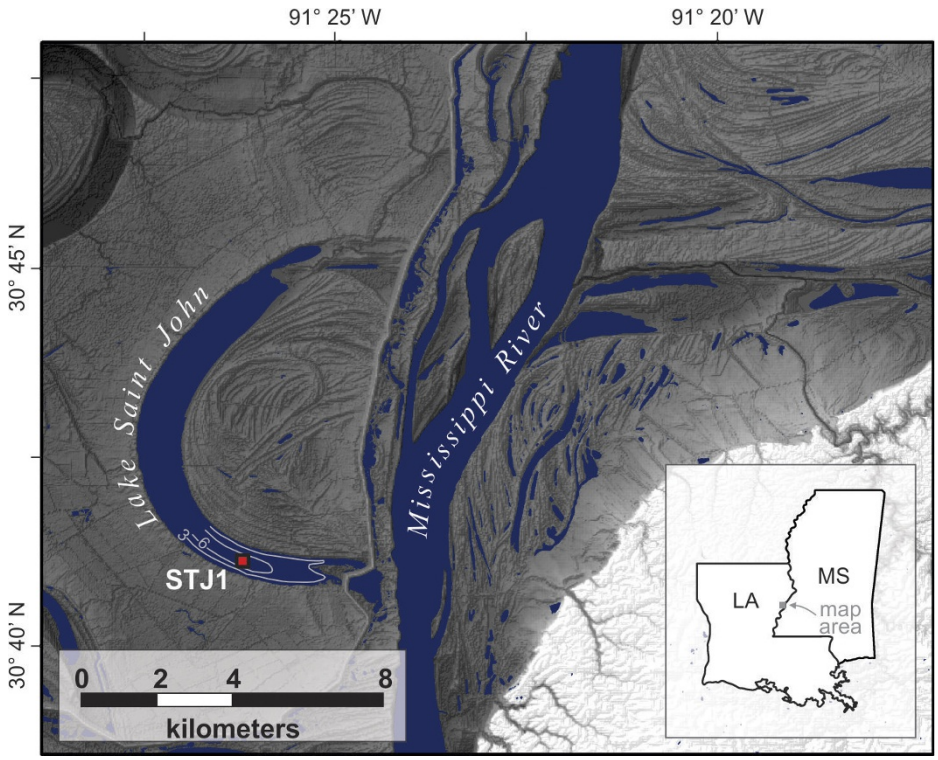

Extended Data Figure 3 | Location of Lake Saint John, Louisiana, and sediment core (STJ1) used in this study. Lake Saint John is an oxbow lake that formed via neck cut-off of the lower Mississippi River in about AD 1500[20] and is situated outside the modern floodway. Bathymetric contours (white) given in metres. Shaded relief shows relative topographic lows (dark shades) and highs (light shades) according to the National Elevation Dataset[25].

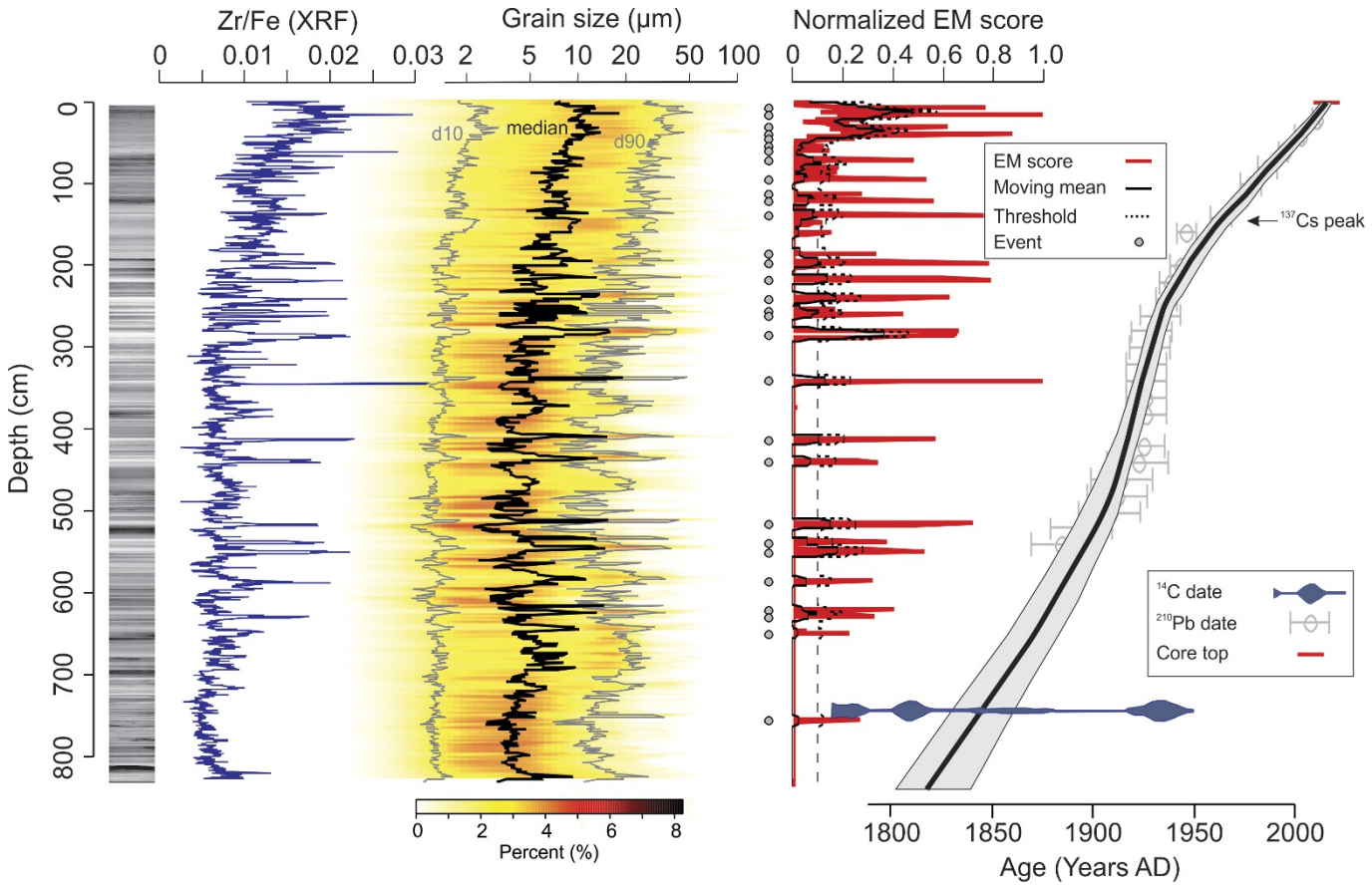

Extended Data Figure 4 | Radiography, bulk geochemistry, grain size and chronology of core MRY2. The age–depth model at right shows the median age probability (black line) and 1σ confidence intervals (grey shading), with 2σ confidence intervals on individual chronological controls.

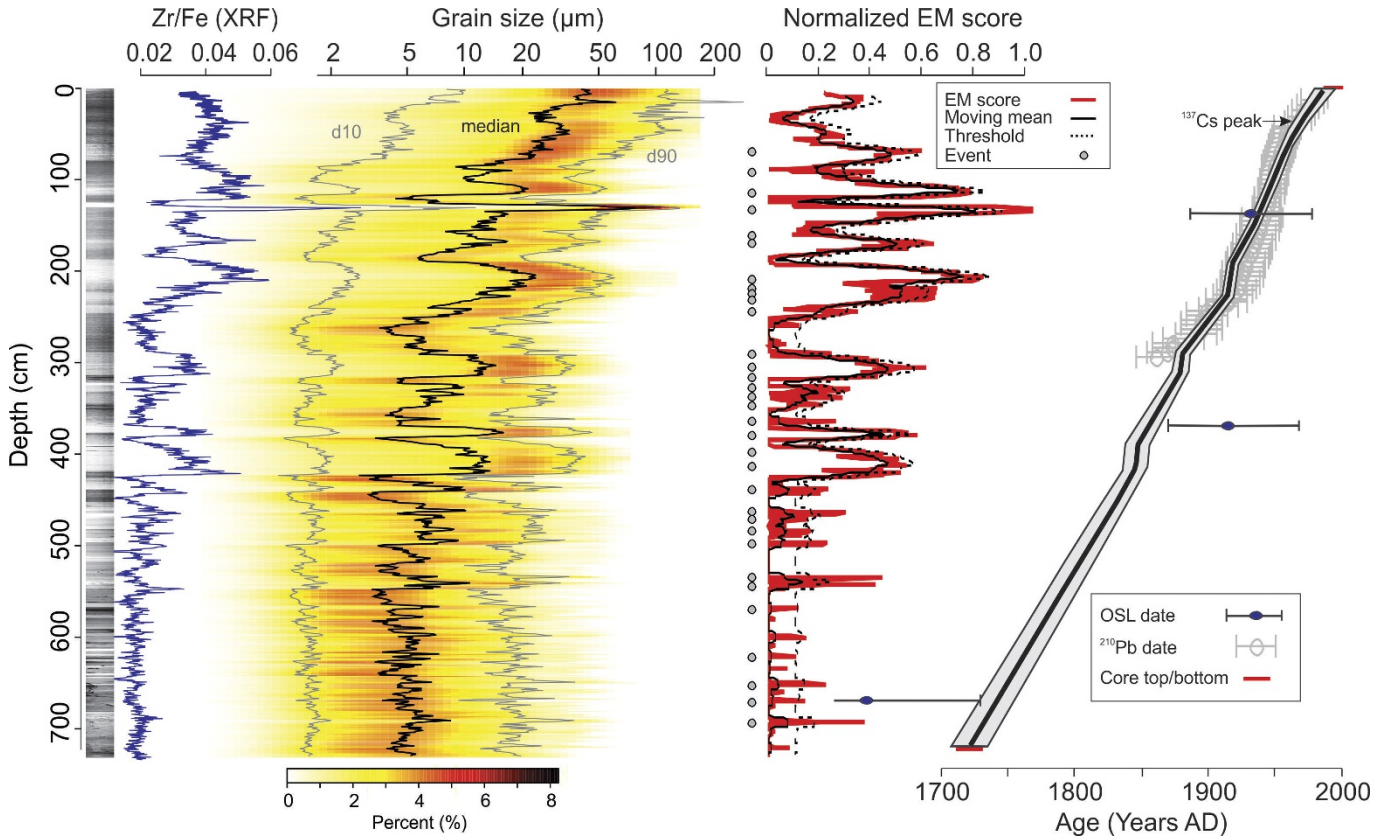

Extended Data Figure 5 | Radiography, bulk geochemistry, grain size and chronology of core FLR1. The age–depth model at right shows the median age probability (black line) and 1σ confidence intervals (grey shading), with 2σ confidence intervals on individual chronological controls.

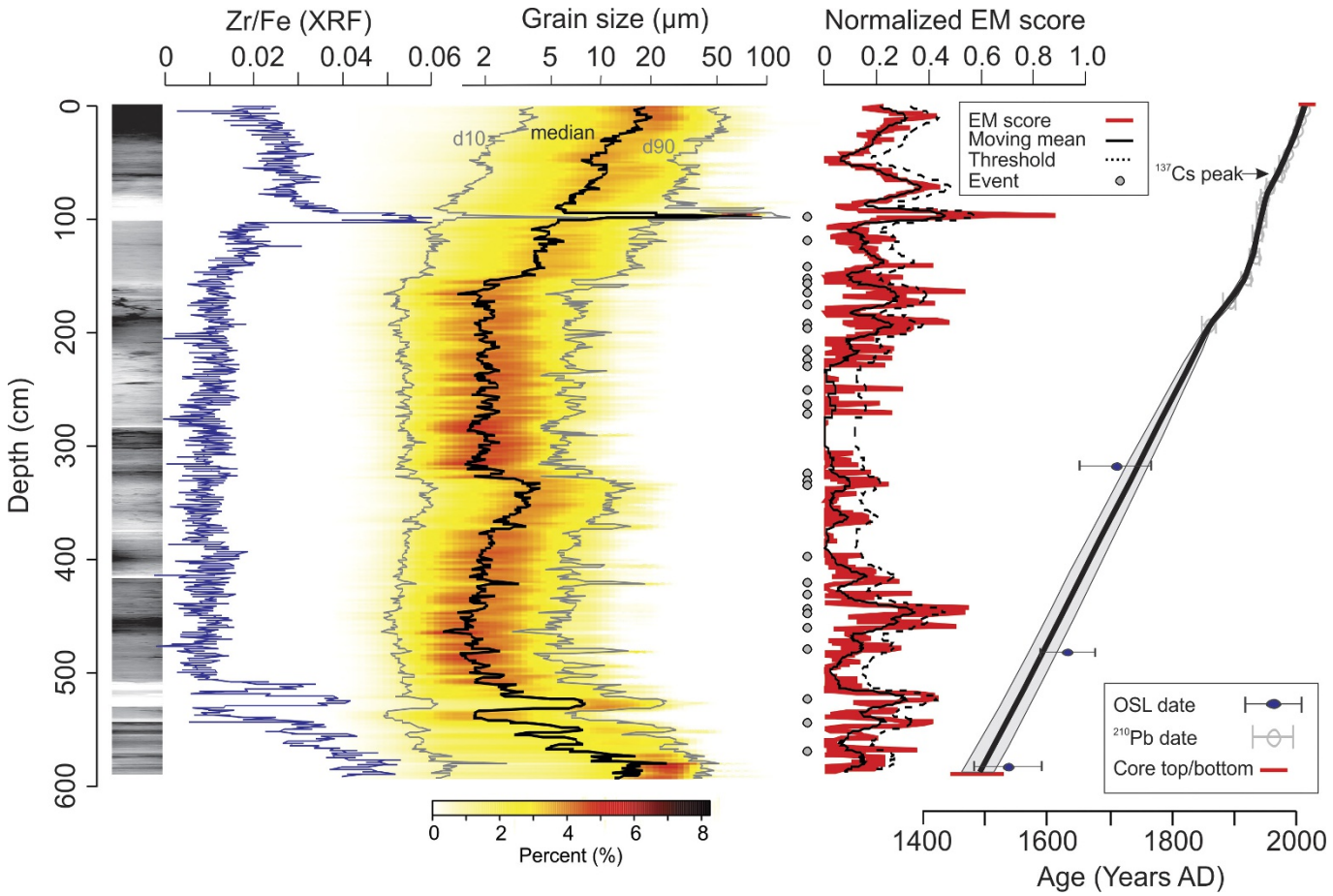

Extended Data Figure 6 | Radiography, bulk geochemistry, grain size and chronology of core STJ1. The age–depth model at right shows the median age probability (black line) and 1σ confidence intervals (grey shading), with 2σ confidence intervals on individual chronological controls.

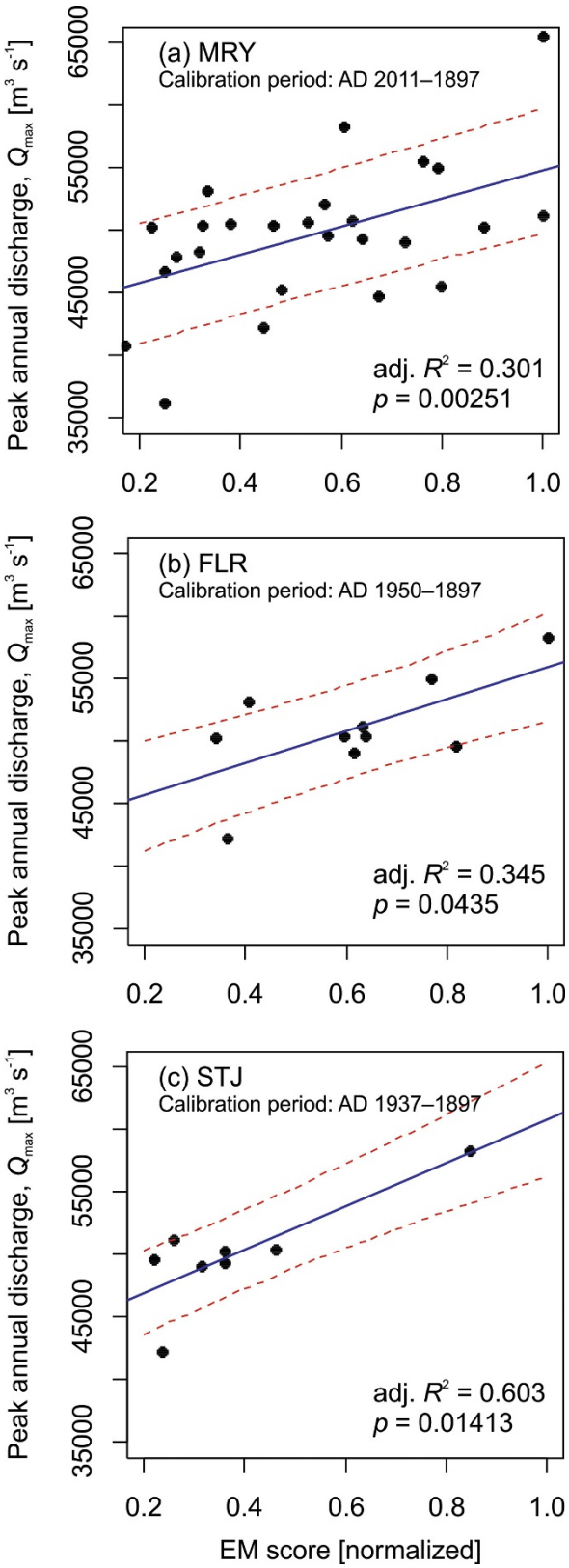

Extended Data Figure 7 | Relationships between peak annual discharge and normalized EM score for historical floods in sedimentary archives. Scatterplots and linear regressions with 1σ prediction intervals relating normalized EM score (a measure of grain size) to peak annual discharge of historical flood events for (**a**) MRY, (**b**) FLR and (**c**) STJ. Peak annual discharge estimates are from the Mississippi River gauging station at Vicksburg. Calibration periods vary owing to site-specific factors discussed in the Methods and Supplementary Information. adj., adjusted.